Met. Mater. Int., Vol. 24, No. 1 (2018), pp. 231~239
doi: 10.1007/s12540-017-7094-x

Microstructure and Crystallographic Texture of Pure Titanium Parts Generated by Laser Additive Manufacturing

Felipe Arias-González[1], Jesús del Val[1], Rafael Comesaña[2], Joaquín Penide[1], Fernando Lusquiños[1], Félix Quintero[1], Antonio Riveiro[1], Mohamed Boutinguiza[1], Francisco Javier Gil[3], and Juan Pou[1,*]

[1]Department of Applied Physics, University of Vigo, EEI, Vigo E-36310, Spain
[2]Department of Materials Engineering, Applied Mechanics and Construction, University of Vigo, EEI, Vigo E-36310, Spain
[3]Department of Materials Science and Metallurgy, Technical University of Catalonia (UPC), ETSEIB, Barcelona E-08028, Spain

(received date: 4 February 2017 / accepted date: 5 June 2017)

In this paper, the microstructure and crystallographic texture of pure Ti thin walls generated by Additive Manufacturing based on Laser Cladding (AMLC) are analyzed in depth. From the results obtained, it is possible to better understand the AMLC process of pure titanium. The microstructure observed in the samples consists of large elongated columnar prior β grains which have grown epitaxially from the substrate to the top, in parallel to the building direction. Within the prior β grains, α-Ti lamellae and lamellar colonies are the result of cooling from above the β-transus temperature. This transformation follows the Burgers relationship and the result is a basket-weave microstructure with a strong crystallographic texture. Finally, a thermal treatment is proposed to transform the microstructure of the as-deposited samples into an equiaxed microstructure of α-Ti grains.

Keywords: laser cladding, metals, powder processing, epitaxy, electron backscatter diffraction (EBSD)

1. INTRODUCTION

Titanium and its alloys are key materials for engineers in a wide range of applications, and specifically, they are strategic materials in the biomedical field [1-3]. Currently, commercially pure titanium (cp-Ti) grades 1, 2, 3, and 4, Ti6Al4V and Ti6Al4V ELI are successful biomaterials employed for the replacement of hard tissues [4]. They present higher biocompatibility, higher corrosion resistance, and a relatively lower elastic modulus compared to other metallic biomaterials.

Additive Manufacturing (AM) of titanium and its alloys increasingly attract more and more attention due to their application to medicine [5,6]. AM is a group of technologies to generate 3D objects by adding layer-upon-layer of material. The application of this technique in the industry is particularly suitable for producing low volumes of products, parts with complex geometries and customized components.

AMLC is a process to build up a metallic or ceramic component by depositing material layer by layer in a continuous manner [7-11]. There are other similar techniques, which are known under different names and acronyms: Laser Engineering Net Shaping (LENS) [12], Laser Powder Deposition (LPD) [13], Direct Metal Deposition (DMD) [14], Laser Consolidation (LC) [15], Direct Laser Deposition (DLD) [16], etc.

In AMLC, the laser beam is employed as a heat source to generate a molten pool in a substrate; and the precursor material, in the form of particles or wire, is fed into the molten pool. The relative movement between the laser head and the workpiece makes possible to deposit material to generate single tracks with dimensions of millimeters or microns [13,17-20]. The overlapping of single tracks allows creating a bidimensional layer, and by stacking layers is possible to build up a part.

Particularly, AM of Ti6Al4V has been widely studied because it is the most commonly used titanium alloy in bioimplants and even in all the industry. It is possible to find research work studying the microstructure and crystallographic texture of Ti6Al4V parts generated by Shape Metal Deposition [21]; by Electron Beam Melting [22-25]; by Selective Laser Melting [25-27]; and by AMLC or similar techniques [14,16,19,28-32].

Although Ti6Al4V is the most commonly used titanium alloy, cp-Ti can be employed in any application where corrosion resistance, strength, and corrosion fatigue resistance are important. As an example, almost all commercially available dental implants are made of cp-Ti [4,6]. Research work on AM of cp-Ti is not as abundant as in the case of Ti6Al4V. LENS technique has been employed to generate porous Ti implants and evaluate their biocompatibility [12], cp-Ti grade 2 has

*Corresponding author: jpou@uvigo.es

been used as a precursor material to study a novel Laser Powder Microdeposition system [13], and AMLC has been studied to produce thin walls of pure Ti [9]. However, an in-depth analysis of the microstructure and crystallographic texture obtained in the pure titanium parts has not been tackled in these works.

Microstructures obtained in AMLC are the consequence of complex thermal cycling: material is melted and rapidly cooled repeatedly during the process, which also implies several phase transformations cycles. The observation of the final microstructure obtained in the pure Ti parts is interesting to fully understand the process. Besides, it has been demonstrated that crystallographic texture plays an important role in the use of pure titanium as an orthopedic biomaterial, because it affects the mechanical properties, corrosion behavior, cell proliferation and osteogenesis [33].

In this work, the microstructure and crystallographic texture obtained in the pure Ti thin walls generated by AMLC is studied in depth. The microstructure was studied by Optical Microscopy (OM) and Scanning Electron Microscopy (SEM); composition by X-Ray Diffraction (XRD); and crystallographic texture was studied via Electron Backscatter Diffraction (EBSD).

2. EXPERIMENTAL PROCEDURE

AMLC technique was selected to produce pure titanium parts (see Fig. 1(a)). The experiments were performed employing a high power fiber laser (SPI SP-200C) to generate the molten pool. The laser beam was focused on the substrate by a lens with a diameter of 50 mm and a focal length of 120 mm, obtaining a circular spot with a diameter of approximately 60 μm on the surface of the substrate. The mean irradiance was 35.4 kW/mm^2 for a delivered laser power of 100 W, in continuous mode.

A CNC table was employed to move the substrate with regard to the laser head. The metallic substrate moves at 5 mm/s with regard to the laser beam and particle injector, generating the first clad. When it reaches the end, the substrate is moved down one step (50 μm) and starts the movement in the opposite direction to create a new overlaid clad. This sequence of movements is performed continuously in a loop and a sample of several millimeters in height is built, layer by layer. The samples were generated by depositing 400 layers continuously with a step between layers of 50 μm (see Fig. 1(b)).

Commercially pure Ti grade 4 powder, Metco 4017 from Oerlicon Metco was used as a precursor material to generate the samples. As can be seen in Fig. 2, powder is irregular shaped and its size range between 70 μm and 180 μm. Irregular shaped powder has been demonstrated to be viable for producing fully dense and crack free walls by a process similar to AMLC [34-36]. However, the process has been limited to using only gas-atomised, spherical powders. In this paper, the feasibility of

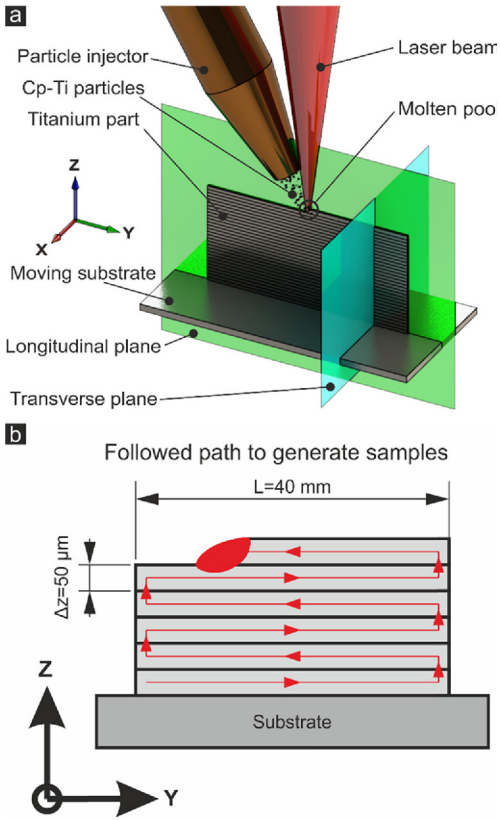

Fig. 1. (a) Sketch of the experimental set-up and (b) Outline of the path followed to generate pure titanium samples.

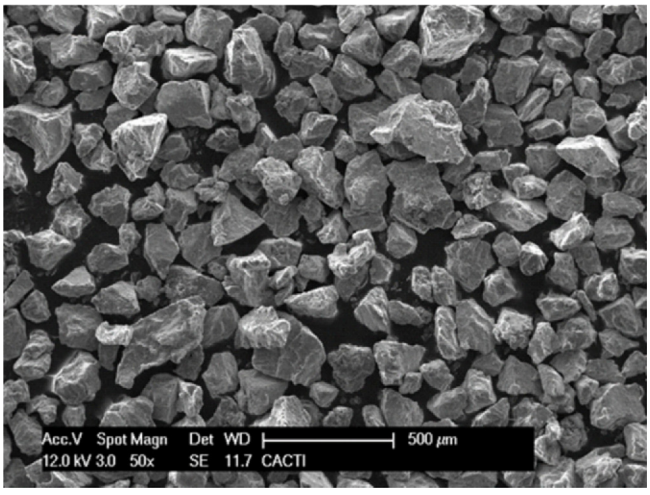

Fig. 2. SEM micrograph showing particle size and morphology of cp-Ti grade 4 particles employed in this work.

using water-atomised powders is investigated, based on an experimental comparison of gas- and water- atomised powders in multiple layer, laser fused deposition of 316L stainless steel. The work shows that, despite much lower cost (approximately 25% of the price of gas-atomised powders. In particular, irregular shaped Ti powder has been successfully employed to produce three-dimensional volumes of pure titanium with-

out pores and cracks by means of AMLC [9].

The powder was carried by argon and laterally injected in the molten pool by a convergent nozzle. The mass flow of cp-Ti grade 4 particles is fixed at a rate of 0.45 g/min. The powder material is melted and distributed layer by layer over the partly built sample. This heated material solidifies in an inert atmosphere when the laser beam goes on sweeping a path leaving the interaction zone.

The samples were cut, embedded in epoxy resin and polished in order to examine the transverse section and the longitudinal section. The analysis of the morphology and microstructure was done by optical microscopy, after etching the samples with Kroll's reagent. The microstructure was also studied by means of scanning electron microscopy (SEM, Philips XL30) employing a backscattering electron detection mode. The qualitative elemental composition was determined via Energy-dispersive X-ray spectroscopy (EDS, EDAX PV9760 coupled to the SEM).

X-Ray Diffraction (XRD) analysis was carried out by means of a PANalytical X'Pert Pro X-ray diffractometer, using monochromated Cu-Kα radiation (λ = 1.54 Å) over the 10-90° 2θ range with a step size of 0.02°. Diffractograms were obtained directly from the polished surface of the longitudinal section. It was done to compare the crystal structure of the samples with the cp-Ti grade 4 particles. The crystallographic texture was analyzed by Electron Backscatter Diffraction (EBSD, Oxford HKL Channel 5 detector equipped on a dual-beam workstation FEI HELIOS 600 NanoLab).

Finally, a set of samples were thermally treated to transform the microstructure of the as-deposited samples into an equiaxed microstructure of α-Ti grains. The chosen thermal treatment was to increase the temperature of the samples slightly above βtransus, 934 °C [37], and slowly cool them in the furnace from the β domain. More specifically, the temperature was increased up to 1000 °C at a rate of 10 °C/min, the holding time was 30 min and the cooling was done at a rate of -15 °C/min. This thermal treatment was carried in vacuum to prevent the oxidation (10^{-3} Pa). The longitudinal sections of these samples were polished and etched with Kroll's reagent. They were observed by optical microscopy to compare the microstructure before the thermal treatment (in the as-deposited samples) and after it.

3. RESULTS AND DISCUSSION

Three-dimensional simple parts have been generated with a transverse dimension below 1 mm (0.7 mm) and a height of 20 mm (see Fig. 3(a)). The transverse section of the samples presents a lamellar microstructure, also known as basket-weave structure (see Fig. 3(b)). The finest lamellae are present at the bottom of the samples (Fig 3(c)); looking towards the top, the lamellae become longer and organized into bigger colonies (Figs. 3(d), 3(e), and 3(f)). The basket-weave microstructure is typically obtained as a result of simple cooling from temperatures above the β-transus of cp-Ti grade 4: 934 °C [37]. When the temperature falls below the transus temperature, β-Ti (BCC) transforms into α-Ti (HCP) lamellae into the prior β grain. However, at very high cooling rates (faster than 350 K/s) from temperatures above the martensite start temperature of cp-Ti grade 4, Ms=850 °C [37], β-Ti (BCC) transforms into α'-Ti (HCP) by a diffusionless transformation process that results into a microstructure apparently similar.

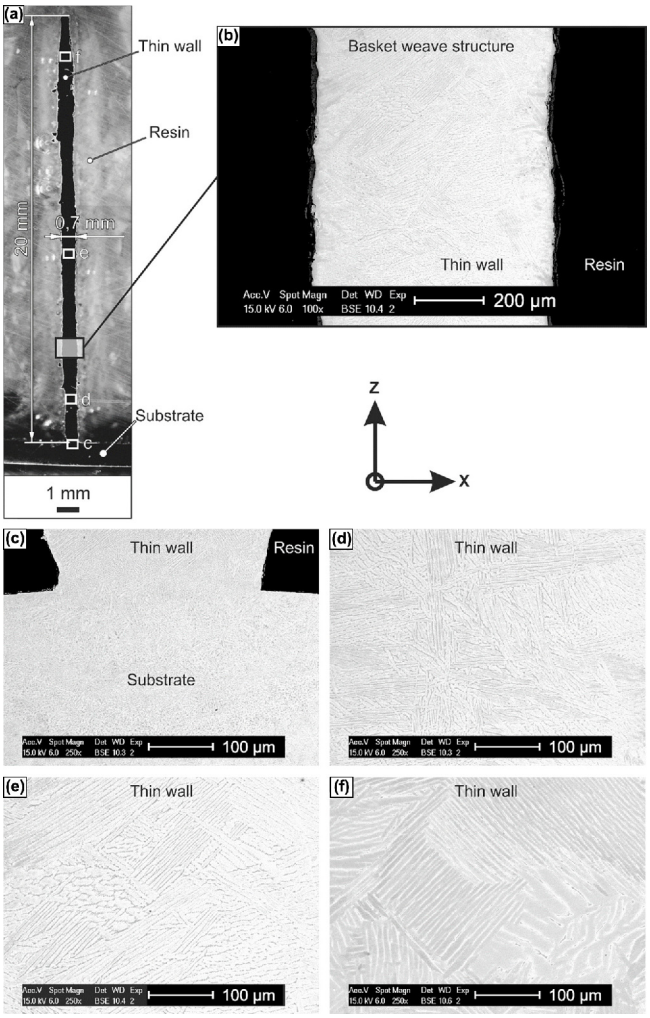

Fig. 3. (a) Optical micrograph showing a transverse section of pure titanium sample and (b-f) SEM micrographs obtained at different heights in the transverse section of the sample.

Laser Cladding and AMLC are characterized by high cooling rates of the deposited material [38-41]. The cooling rate, at a given location near the molten pool, can be calculated by multiplying the thermal gradient at the liquidus isotherm and the beam scanning speed (5 mm/s) [41]. Thermal gradient across the molten pool in similar processes is reported to be between 10^5 K/m and 10^6 K/m [39,41,42]. A decrease in the layer thickness and the deposition rate of material produce an increase in the thermal gradient and the cooling rates [38].

The thickness of the individual layers employed to generate our samples is 50 μm, which is smaller than the ones reported in those studies. Therefore, we consider the gradient across the molten pool to be in the order of 10^6 K/m. Moreover, the width of the sample is below 1 mm, so the molten pool and heat affected zone during the process have a size in the order of millimeters. In the molten pool and the heat affected zone, the temperature changes from highly above the melting point (1660 °C) to below the β-transus (934 °C). There exists a difference in temperature of more than 1000 K in a distance in the order of 1 mm. Therefore, it is realistic considering a temperature gradient across the molten pool in the order of 10^6 K/m. The cooling rate is calculated to be in the order of 5000 K/s by multiplying the estimated thermal gradient (10^6 K/m) and the beam scanning speed (5 mm/s). However, to take into account the inaccuracy in the estimation of the thermal gradient, we consider a broad range so the cooling rate is estimated to be in the order of 10^3-10^4 K/s.

Since the estimated cooling rate is higher than 350 K/s, the microstructure should be the result of a diffusionless transformation from β-Ti (BCC) to α'-Ti (HCP). However, long and thick lamellae organized into colonies are observed, especially, in Figs. 3(e) and 3(f). These microstructures are identified as thin (Fig. 3(d)) and thick (Figs. 3(e) and 3(f)) lamellar microstructures with α phase. Therefore, they are not the result of a rapid cooling from above β-transus and the phase transformation might be attributed to a diffusional process. The obtained microstructures are the consequence of a complex thermal cycling which also implies several phase transformations cycles. During the deposition process, titanium is melted and rapidly cooled down. However, when new layers of material are generated, the previously deposited titanium is remelted and rapidly cooled again more times. After depositing more new layers, part of the material is not remelted anymore, but it is still heated and cooled several more times. Besides, the cooling rate changes while the part is being built because it is mainly produced by heat conduction from the molten pool to the substrate. In the first layers, the cooling rates are higher resulting in a finer microstructure. When new layers are added the distance from the molten pool to the substrate increases. Therefore, the heat conduction resistance is higher and the heat evacuation from the molten material to the substrate decreases. The result is a lower cooling rate and the formation of the bigger lamellar colonies observed in the top of the samples.

XRD analysis was performed to compare the diffractogram of precursor material, cp-Ti grade 4 particles (Fig. 4(a)) and the diffractogram obtained in the longitudinal section of the samples (Fig. 4(b)). The diffractogram of precursor material perfectly matches the pattern of α-Ti (HCP). However, some peaks are missing in the XRD of the samples, indicating a microstructure with preferential orientation of the crystal structure.

In order to fully understand the crystal structure of the samples, they were etched with Kroll's reagent to observe their longitudinal section under the optical microscope (Fig. 5(a)). Samples present a microstructure formed by large elongated columnar prior β grains emerging from the substrate to the top, parallel to the building direction (Z axis in Fig. 5). This structure is the result of an epitaxial growth from the parent grains during solidification of the molten pool [43] thus leading to large temperature gradients. This is used, in unison with closely controlled solidification velocities, to stabilise the columnar dendritic growth, thereby avoiding nucleation and growth of equiaxed grains in the laser clad. It is possible with this technique to deposit a single crystal clad by epitaxial growth onto a single crystal substrate. In this paper, the microstructure obtained by E-LMF is analysed by scanning electron microscopy (SEM. A low mass deposition rate and an excess of laser power delivered results in a large penetration of the molten pool. It produces a remelting of the previously deposited layers and promotes the formation of columnar grains via bottom grain epitaxial growth [44].

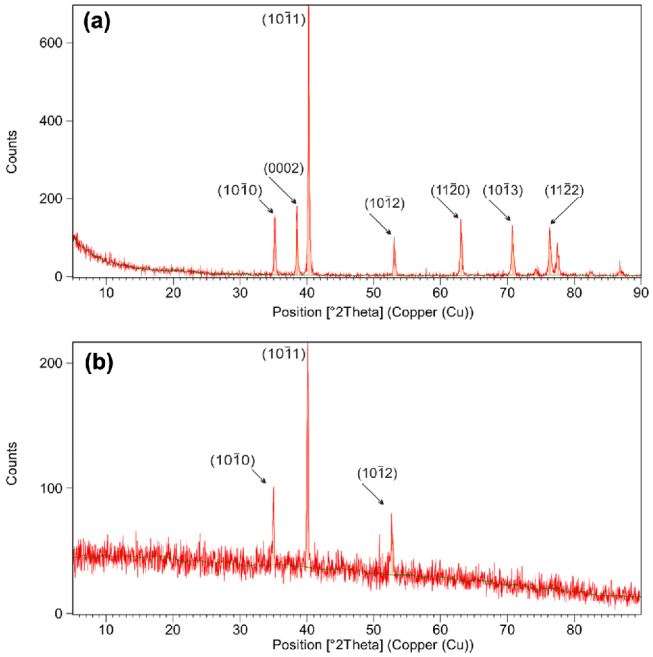

Fig. 4. Comparative of X-ray diffractograms; (a) cp-Ti grade 4 particles (precursor material) and (b) longitudinal section of the pure titanium part (AMLC sample).

EBSD analysis was done in three areas at different heights to study the microstructure and crystallographic texture along one columnar grain (Fig. 5(a)). EBSD maps are colored codifying Euler angles into RGB values for each pixel. The changes in the size of the lamellae and colonies are clearly observed again in the EBSD maps (Figs. 5(b), 5(c), and 5(d)). As it was reported in the study by SEM (Fig. 3), the longitude of lamellae and colonies increase from the bottom to the top of the samples. In the EBSD maps, each color corresponds to a crystallographic orientation and it is possible to discern 6 pre-

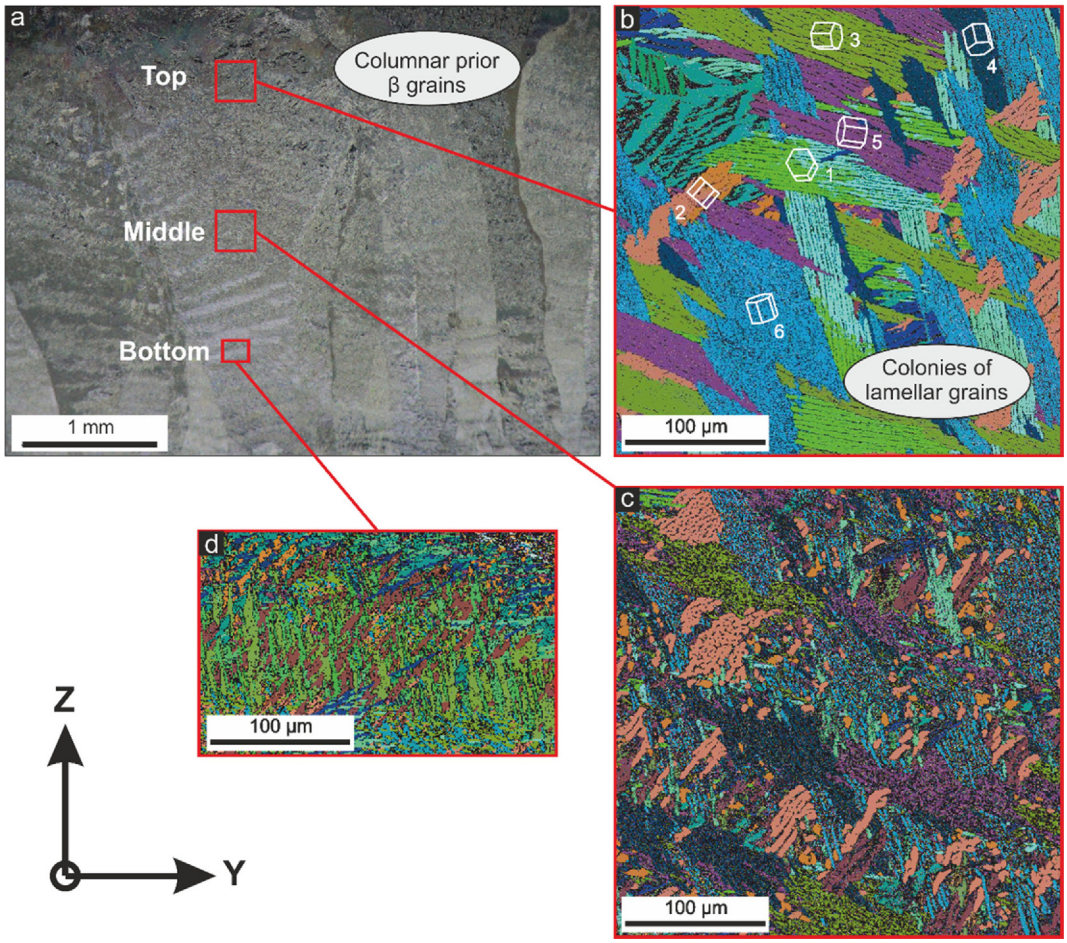

Fig. 5. (a) Optical micrograph showing a longitudinal section of pure titanium sample and (b-d) EBSD maps colored codifying Euler angles into RGB values for each pixel.

ferred orientations in Fig. 5(b). However, to discern the preferred orientations more accurately is necessary to analyze the pole figures.

The crystallographic texture can be fully understood by studying pole figures obtained for each EBSD map (Fig. 6). Pole figures present the same pattern along all the columnar grain. The observed crystallographic texture results of the transformation of β-Ti (BCC) into αTi (HCP) produced when the material is cooled. During the β to α transformation, the BCC plane (110)β transforms to the basal plane (0001)α of the hexagonal phase according to the Burgers orientation relationship [2]. There exist six possible (110)β planes in a cubic crystal that correspond to the six preferred orientations of the (0001)α planes in the pole figures. The pole figure of the basal planes (0001)α is reminiscent of the pattern (110)β in the prior BCC crystallographic orientation.

Among that, for each orientation of the (110)β // (0001)α plane, there exist two possible slip directions <111>β, which become <11-20>α direction after the transformation from β-Ti (BCC) to αTi (HCP). For every basal plane (0001)α there are two possible sets of <11-20>α reflections. These two crystallographic orientations for each basal plane form an angle of 10.5º between them [21]manufactured by shaped metal deposition (SMD. In the pole figures (Fig. 6) for the type I prismatic plane, (10-10)α, and type II prismatic plane, (11-20)α, there are pairs of adjacent poles (separated around 10º). Therefore, samples present all the twelve possible crystallographic orientations into the prior β grain: six orientations of the basal plane (0001)α and, for each one, two sets of <11-20>α reflections. For the same basal plane, the two possible crystallographic orientations are very similar and it is not possible to discern them clearly in the EBSD maps attending to their coloring (Fig. 6).

The EBSD maps also show a significant amount of pixels that were not indexed. Figure 7(a) is the EBSD map of a small area in the longitudinal section to analyze this issue in detail. Those colored pixels that correspond to the lamellae, present a well-defined EBSD pattern (Fig. 7(b)). However, in the inter-lamellae space the signal strength is low and the pattern is not well defined (Fig. 7(c)), which can be due to an amorphous structure or a highly distorted crystal lattice. This fact is in accordance the wide band present in the XRD spectrum of the samples (Fig. 4(b)). During the transformation of the β-Ti (BCC)

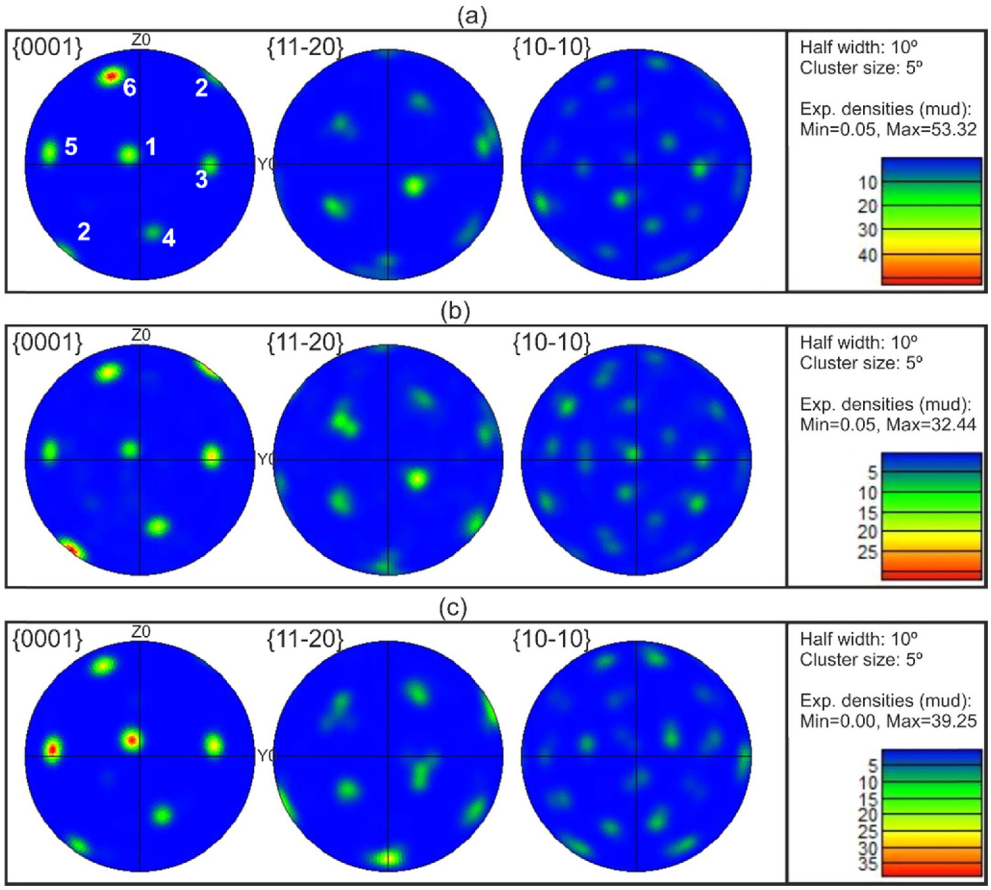

Fig. 6. Basal {0001}, Prism type I {10-10} and Prism type II {11-20} pole figures corresponding to the (a) top, (b) middle, and (c) bottom EBSD maps of Fig. 5.

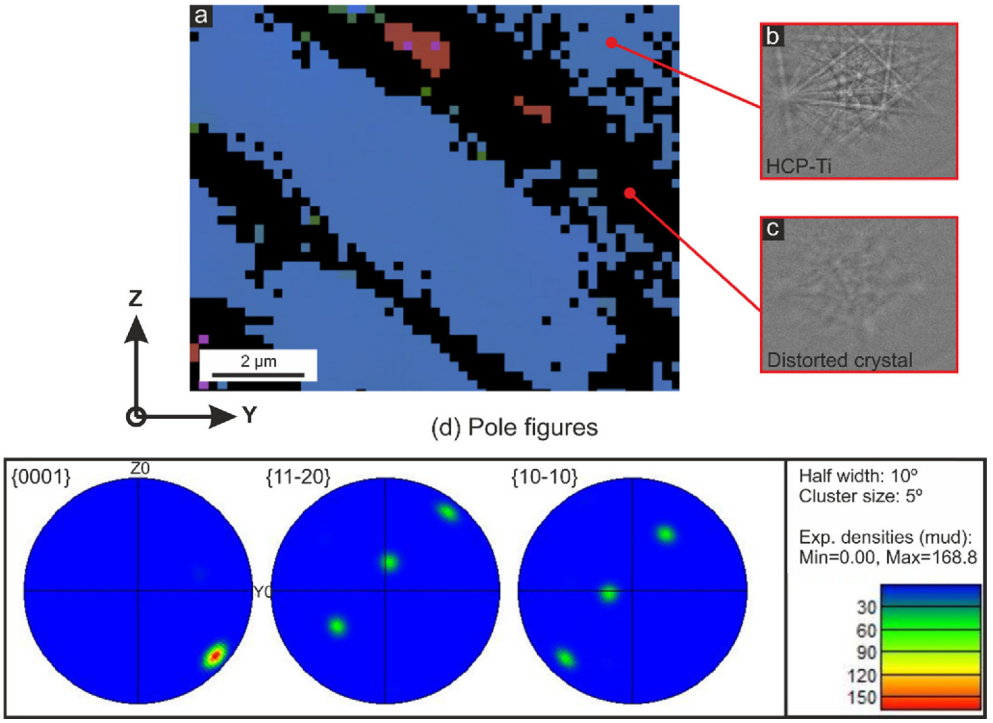

Fig. 7. (a) EBSD map of small area in the longitudinal section of the sample, (b) EBSD pattern in a lamella, (c) EBSD pattern in an inter-lamellae space, and (d) Pole figures of the EBSD map.

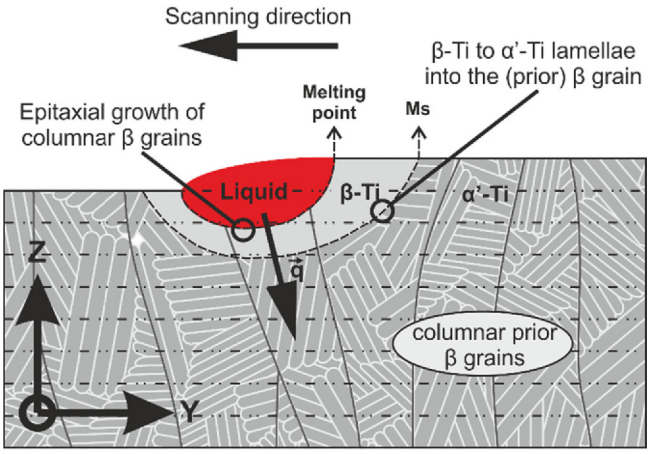

Fig. 8. Sketch to illustrate the formation of the microstructure and crystallographic texture of the samples.

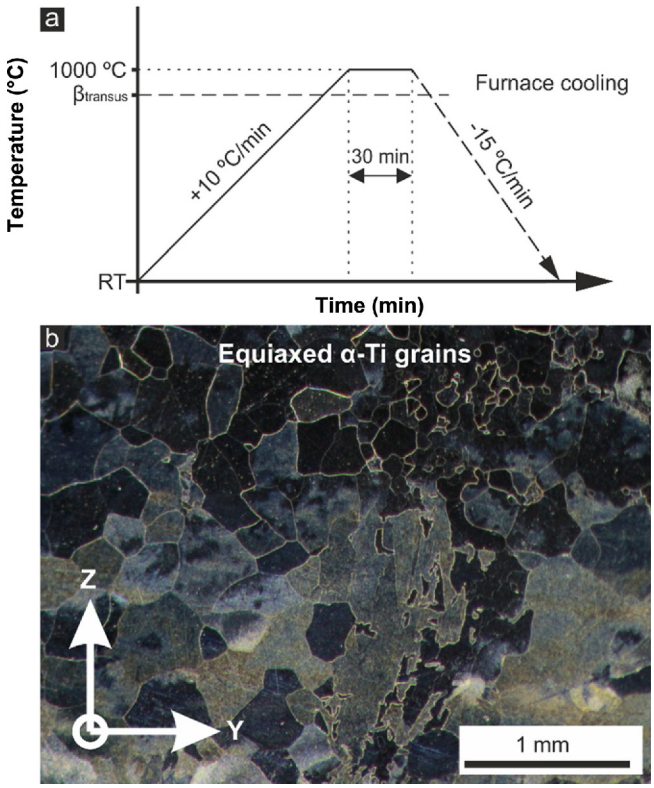

Fig. 9. (a) Thermal treatment of samples after deposition and (b) Optical micrograph showing a longitudinal section of pure titanium sample thermally treated.

to α-Ti (HCP), the plane (334)β does not suffer distortion and it becomes the (41-50)α [37]. The transformation produces great distortions in the perpendicular direction to this plane causing the appearance of this interlamellae spaces with an amorphous or highly distorted crystal structure. The colonies are sandwich-structured formed by alternating lamellae and inter-lamellae spaces parallel to the (41-50)α plane.

From the results obtained, it is possible to better understand the AMLC process of pure titanium (Fig. 8). During the process, previously deposited layers of material are remelted. When the laser beam leaves the interaction zone, the cooling is produced mainly by heat conduction to the already built part (and substrate). Therefore, the boundary between the molten pool and the previously deposited layers is a solidification front; where an epitaxial growth of columnar β grains takes place mimicking the crystallographic orientation of the previously deposited layers. When the material is cooled below β-transus, β-Ti (BCC) is transformed into αTi (HCP). This transformation follows the Burgers relationship [2] giving, as a maximum, twelve variants of crystallographic orientation to the α-Ti into each prior β columnar grain. Consequently, the microstructure consists of elongated prior β columnar grains formed by α-Ti lamellae and lamellar colonies structured in a basket-weave pattern with a strong crystallographic texture.

Finally, a set of samples were thermally treated in vacuum following the sequence represented in Fig. 9(a). The thermal treatment was chosen to transform the microstructure of the samples into equiaxed α-Ti grains. The thermal treatment consisted of increasing the temperature of the samples slightly above β-transus and slowly cool them in the furnace from the β domain. Figure 9(b) is an optical micrograph showing the longitudinal section of a thermally treated sample. In comparison with original microstructure (Fig. 5(a)), columnar prior β grains have disappeared. When the samples are heated above β-transus the microstructure of the as-deposited samples is transformed into new β grains. Slow cooling from the β domain (above βtransus) produces a transformation from βTi (BCC) to α-Ti (HCP), resulting in the equiaxed structure of α-Ti grains showed in Fig. 9(b).

4. CONCLUSION

An in-depth analysis of the microstructure and crystallographic texture obtained in the pure Ti thin walls generated by AMLC was presented. The microstructure consists of large elongated columnar prior β grains emerging from the substrate to the top, in parallel to the building direction. The prior β grains are formed by α-Ti lamellae and lamellar colonies, which are structured in a basket-weave pattern.

The prior β columnar grains are produced by an epitaxial growth from the parent grains during solidification of the molten pool. Employing a low mass deposition rate and an excess of laser power, previously deposited layers of material are remelted. When the laser leaves the interaction zone, an epitaxial growth of columnar β grains is produced in the solidification front. The newly solidified material mimics the crystallographic orientation of the previously deposited layers.

Within the prior β grains, α-Ti lamellae structure is the result of cooling from above the β-transus temperature. This transforma-

tion follows the Burgers relationship and α-Ti lamellae present twelve variants of crystallographic orientation into each prior β grain. The result is a basket-weave microstructure with a strong crystallographic texture. The finest lamellae are present in the bottom part of the samples and towards the top, the lamellae are longer and organized into bigger colonies. This phenomenon is caused by a reduction in the cooling rate while the part is being built.

A thermal treatment can be applied to transform the microstructure of the as-deposited parts into an equiaxed microstructure of α-Ti grains. The thermal treatment proposed consisted of increasing the temperature of the samples slightly above β-transus and slowly cool them in the furnace from the β domain. Heating the parts above β-transus eliminates the large elongated columnar prior β grains and the slow cooling from the β domain gives as a result the equiaxed α-Ti grains microstructure.

ACKNOWLEDGMENTS

This work was partially supported by Government of Spain (MAT2015-71459-C2-P), FPU program FPU13/02944 grant, Xunta de Galicia (CN2012/292, POS-A/2013/161, and ED481B 2016/047-0) and the University of Vigo (Research Grant F. Arias-González). The authors wish to thank the technical staff from CACTI (University of Vigo) for their technical assistance.

REFERENCES

1. M. J. Donachie, *Titanium: A Technical Guide, 2nd ed.*, pp.5-11, ASM International, Materials Park, Ohio, USA (2000).
2. C. Leyens and M. Peters, *Titanium and Titanium Alloys*, pp.423-466, Wiley-VCH Verlag GmbH & Co. KGaA, Weinheim, Germany (2003).
3. I. P. Polmear, *Light Alloys: From Traditional Alloys to Nanocrystals, 4th ed.*, pp.299-366, Elsevier/Butterworth-Heinemann, Oxford, UK (2006).
4. Y. Oshida, *Bioscience and Bioengineering of Titanium Materials*, pp.217-256, Elsevier, Oxford, UK (2007).
5. N. Guo and M. C. Leu, *Front. Mech. Eng.* **8**, 215 (2013).
6. A. Sidambe, *Materials (Basel)* **7**, 8168 (2014).
7. R. Comesaña, F. Lusquiños, J. del Val, M. López-Álvarez, F. Quintero, J. Pou, *et al. Acta Biomater.* **7**, 3476 (2011).
8. R. Comesaña, F. Lusquiños, J. del Val, T. Malot, M. López-Álvarez, J. Pou, *et al. J. Eur. Ceram. Soc.* **31**, 29 (2011).
9. F. Arias-González, J. del Val, R. Comesaña, F. Lusquiños, F. Quintero, J. Pou, *et al. 8th Iberoamerican Optics Meeting and 11th Latin American Meeting on Optics, Lasers, and Applications* (ed. M. F. P. C. Martins Costa), p. 878546, SPIE, Porto, Portugal (2013).
10. R. Comesaña, F. Lusquiños, J. del Val, F. Quintero, A. Riveiro, J. Pou, *et al. Sci. Rep.* **5**, 10677 (2015).
11. R. Comesaña, F. Lusquiños, J. del Val, M. López-Álvarez, F. Quintero, J. Pou, *et al. Ceram. Int.* **42**, 2021 (2016).
12. W. Xue, B. V. Krishna, A. Bandyopadhyay, and S. Bose, *Acta Biomater.* **3**, 1007 (2007).
13. C. Meacock and R. Vilar, *Mater. Design* **29**, 353 (2008).
14. G. P. Dinda, L. Song, and J. Mazumder, *Metall. Mater. Trans. A* **39**, 2914 (2008).
15. J. Chen, L. Xue, and S. H. Wang, *J. Mater. Sci.* **46**, 5859 (2011).
16. D. Clark, M. T. Whittaker, and M. R. Bache, *Metall. Mater. Trans. B* **43**, 388 (2012).
17. F. Lusquiños, R. Comesaña, A. Riveiro, F. Quintero, and J. Pou, *Surf. Coat. Technol.* **203**, 1933 (2009).
18. J. del Val, R. Comesaña, F. Lusquiños, M. Boutinguiza, A. Riveiro, J. Pou, *et al. Surf. Coat. Technol.* **204**, 1957 (2010).
19. B. Yao, X. L. Ma, F. Lin, and W. J. Ge, *Rare Metals* **34**, 445 (2015).
20. F. Arias-González, J. del Val, R. Comesaña, J. Penide, F. Lusquiños, J. Pou, *et al. Appl. Surf. Sci.* **374**, 197 (2016).
21. B. Baufeld, O. Van Der Biest, and S. Dillien, *Metall. Mater. Trans. A* **41**, 1917 (2010).
22. S. S. Al-Bermani, M. L. Blackmore, W. Zhang, and I. Todd, *Metall. Mater. Trans. A* **41**, 3422 (2010).
23. A. Safdar, L. Y. Wei, A. Snis, and Z. Lai, *Mater. Charact.* **65**, 8 (2012).
24. A. A. Antonysamy, J. Meyer, and P. B. Prangnell, *Mater. Charact.* **84**, 153 (2013).
25. H. K. Rafi, N. V. Karthik, H. Gong, T. L. Starr, and B. E. Stucker, *J. Mater. Eng. Perform.* **22**, 3872 (2013).
26. M. Simonelli, Y. Y. Tse, and C. Tuck, *Metall. Mater. Trans. A* **45**, 2863 (2014).
27. M. Simonelli, Y. Y. Tse, and C. Tuck, *J. Mater. Res.* **29**, 1 (2014).
28. P. Kobryn and S. Semiatin, *J. Mater. Process. Technol.* **135**, 330 (2003).
29. X. Wu, J. Liang, J. Mei, C. Mitchell, P. S. Goodwin, and W. Voice, *Mater. Design* **25**, 137 (2004).
30. S. H. Mok, G. Bi, J. Folkes, and I. Pashby, *Surf. Coat. Technol.* **202**, 3933 (2008).
31. S. H. Mok, G. Bi, J. Folkes, I. Pashby, and J. Segal, *Surf. Coat. Technol.* **202**, 4613 (2008).
32. C. Qiu, G. A. Ravi, C. Dance, A. Ranson, S. Dilworth, and M. M. Attallah, *J. Alloy. Compd.* **629**, 351 (2015).
33. S. Bahl, S. Suwas, and K. Chatterjee, *RSC Adv.* **4**, 38078 (2014).
34. A. J. Pinkerton and L. Li, *CIRP Ann. - Manuf. Techn.* **52**, 181 (2003).
35. A. J. Pinkerton and L. Li, *Thin Solid Films* **453-454**, 600 (2004).
36. A. J. Pinkerton and L. Li, *Int. J. Adv. Manuf. Tech.* **25**, 471 (2005).
37. M. S. Oh, J. Y. Lee, and J. K. Park, *Metall. Mater. Trans. A* **35**, 3071 (2004).
38. J. Mazumder, A. Schifferer, and J. Choi, *Mater. Res. Innov.* **3**, 118 (1999).
39. R. Ye, J. E. Smugeresky, B. Zheng, Y. Zhou, and E. J. Lavernia, *Mat. Sci. Eng. A* **428**, 47 (2006).

40. B. Zheng, Y. Zhou, J. E. Smugeresky, J. M. Schoenung, and E. J. Lavernia, *Metall. Mater. Trans. A* **39**, 2228 (2008).
41. S. M. Thompson, L. Bian, N. Shamsaei, and A. Yadollahi, *Addit. Manuf.* **8**, 36 (2015).
42. L. Wang, S. D. Felicelli, and J. E. Craig, *J. Manuf. Sci. Eng.* **131**, 041019 (2009).
43. M. Gäumann, S. Henry, F. Cléton, J. D. Wagnière, and W. Kurz, *Mat. Sci. Eng. A.* **271**, 232 (1999).
44. T. Wang, Y. Y. Zhu, S. Q. Zhang, H. B. Tang, and H. M. Wang, *J. Alloy. Compd.* **632**, 505 (2015).